Microwave Photonic Channelizer With Large Instantaneous Bandwidth Based on AOFS

Xiaoqing Xue, Yu Zhang, Bo Chen, and Yong Zhang

***Abstract*—The microwave photonic channelizer can convert the RF signal into the optical domain for transmission and procession, effectively avoiding the limitation of electronic bottleneck, and realizing the instantaneous reception of ultra-wideband signal or multi-frequency signals, which can be perfectly applied to radar system and electronic warfare. In this paper, a microwave photonic channelizer based on dual-output image-reject mixer is proposed, both the signal path and the local oscillator path are divided into three paths by using an optical coupler. An acousto-optic frequency shifter (AOFS) is used by the optical local oscillator to shift the frequency to the left and right and then enters the image rejection mixer with the signal path. Finally, a 6 GHz bandwidth RF signal is divided into six subchannels with a bandwidth of 1 GHz to achieve simultaneous reception. This scheme needs no optical frequency comb and doubles the channelization efficiency, the image rejection ratio of the sub-channels is about 22 dB, and the spurious-free dynamic range of the system can reach 103.2 dB·Hz$^{2/3}$.**

***Index Terms*—Microwave photonics, phononic channelization, AOFS, image rejection.**

I. Introduction

With the rapid development of broadband wireless communications, radar systems, and electronic warfare, the requirement of reception capability for ultra wideband radio frequency (RF) signals is also increasing [1]–[9]. For example, the military receiver proposed by the US Defense Advanced Research Projects Agency (DARPA) requires that the working bandwidth must be greater than 50 GHz, and the instantaneous bandwidth greater than 5 GHz [7]. However, the traditional microwave receiver is limited by the electronic bottleneck and it is too difficult to achieve such an large instantaneous receiving bandwidth [4]–[15]. Microwave channelization is one of the enabling methods to solve the problem by slicing the broadband RF signals into a number of narrow channels [11], [12].

Benefit from the advantages of large bandwidth, low loss, and immunity to electromagnetic interference, microwave photonic channelizer receiver has attracted the attention of many scholars at home and abroad [12]–[14]. With the rapid development of microwave photonic integration technology, miniaturization and portability of channelized receivers will inevitably be the future development trend [15], [16]. The reported microwave photonic channelization schemes can be divided into two categories. The first category relay on optical frequency comb (OFC) and is currently the most studied. Ref. [9] proposed a scheme using OFC and Fabry-Perot (FP) to achieve the reception of two adjacent channels, however the working frequency range cannot be flexibly tuned and there are very few narrow-band optical filters with high Q factors. Ref. [14] proposed a coherent RF channelizer based on dual OFCs and a multichannel image-reject mixer (IRM), however, the number of sub-channels is limited by the number of comb lines. There are many other channelization schemes based on OFCs [18]–[22]. As we know, the generation of OFCs with high flatness and a large number of comb lines is still a critical problem. Ref. [12] mentioned that the Kerr OFC generated by micro-ring resonator (MRR) can greatly increase the number of comb lines of the OFC. However, Kerr optical frequency comb with a large number of comb lines is costly and difficult to integrate. The second category does not require OFC. Ref. [10] uses two linearly frequency-modulated (LFM) optical pulses with proper time delay to achieve 6 sub-channels reception. But the scheme above faces the problem of poor stability.

In this paper, a microwave photonic channelizer with 6 channels based on AOFS is performed. Our scheme only needs to use Mach-Zehnder modulator (MZM) to realize simple carrier suppression double-sideband modulation (CS-DSB), without generating any OFC. AOFSs shift the frequency of the local oscillator (LO) signals to the left and right, and then send the shifted LO signals to the corresponding mixers to achieve dual output image rejection, and finally the broadband RF signal is divided into 6 sub-channels for output. Compared with Refs. [9], [12], the number of optical filters used in the system is greatly reduced. Compared with Ref. [14], the number of IRMs used for 6 channels reception is also reduced by half. By using the scheme we proposed, the reception capability in 20–26 GHz has been demonstrated, the image rejection ratio is around 24 dB, and the spurious free dynamic range (SFDR) can reach 103.2 dB·Hz$^{2/3}$.

Manuscript received August 2, 2021; accepted August 26, 2021. Date of publication September 1, 2021; date of current version September 15, 2021. This work was supported in part by the Shaanxi Province Natural Science Basic Research Project of China under Grant 2021JM-517, in part by the Shaanxi Provincial Key Research and Development Program of China under Grant 2021NY-213, in part by the Young backbone teacher of Xianyang Normal University of China under Grant XSYGG201605, and in part by the Special Scientific Research Program of Shaanxi Provincial Department of Education of China under Grant 21JK0968. *(Corresponding author: Bo Chen.)*

Xiaoqing Xue, Yu Zhang, and Bo Chen are with the School of Physics and Electronic Engineering, Xianyang Normal University, Xianyang 712000, China (e-mail: chen_bo_16@163.com).

Yong Zhang is with the Xianyang Hengtong Electric Power Design Co., Xianyang 712000, China.

Digital Object Identifier 10.1109/JPHOT.2021.3108842

This work is licensed under a Creative Commons Attribution 4.0 License. For more information, see https://creativecommons.org/licenses/by/4.0/

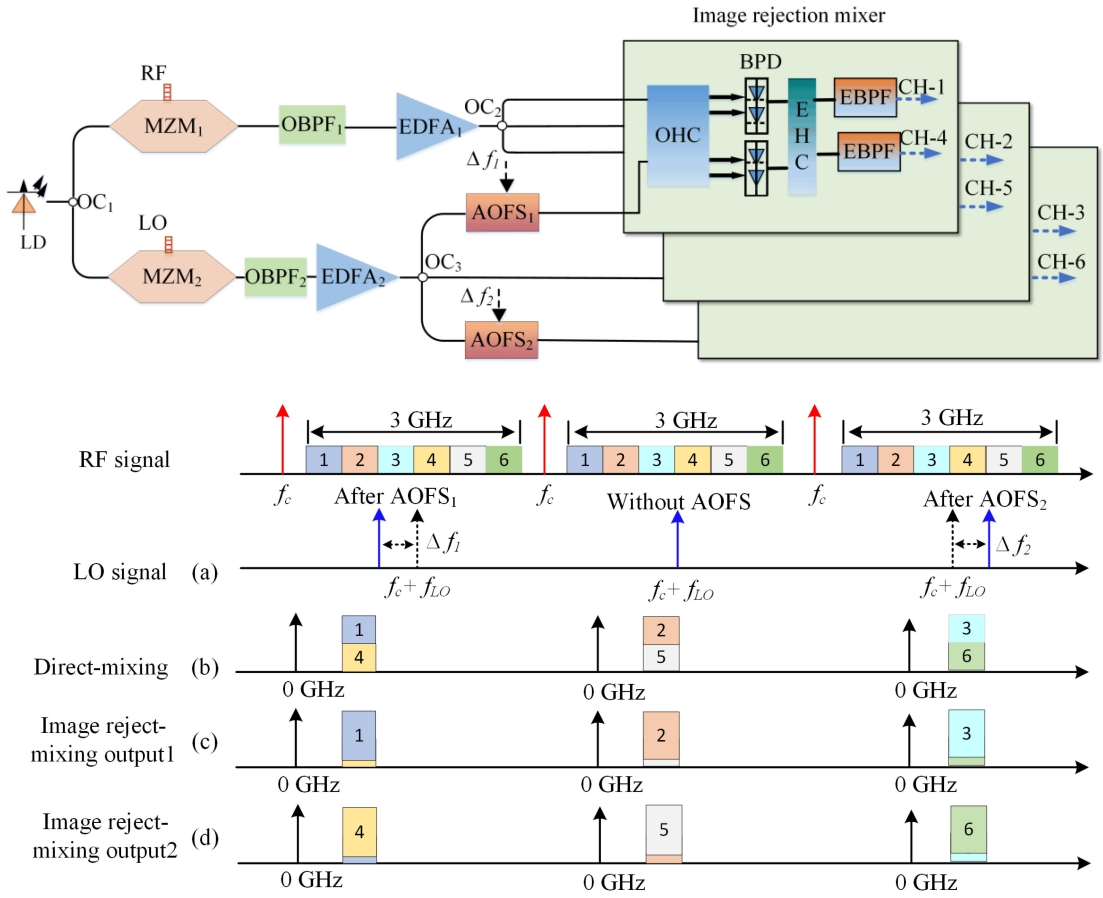

Fig. 1. Schematic diagram of the proposed photonic RF channelizer.

II. Operation Principle

The schematic diagram of the proposed photonic RF channelizer is illustrated in Fig. 1. A continuous optical carrier is generated by a laser diode and divided into upper and lower two branches by the optical coupler (OC_1). In the upper branch, MZM_1 is driven by a wideband RF signal for CS-DSB modulation. The $+1$st order sideband of the RF modulated signal is selected by an optical bandpass filter ($OBPF_1$) and can be expressed as

$$E_{+1st}(t) = 2E_{in}(t)\, J_1(m_1) \exp(j2\pi f_{RF} t) \tag{1}$$

Where $E_{in}(t)$ is the electrical field of the optical carrier, f_{RF} is the frequency of the input wideband RF signal, $J_1(m_1)$ represents the first-order Bessel function, m_1 is the RF modulation index. The output signal from $OBPF_1$ is amplified by $EDFA_1$ and divided into three paths by OC_2 and sent to the corresponding IRMs.

In the lower branch, the MZM_2 is driven by LO signal and also used for CS-DSB modulation. $OBPF_2$ chooses the $+1$st order sideband of the LO modulated signal and sends it into $EDFA_2$ for amplification. The LO signal can be expressed as

$$E_{LO}(t) = 2E_{in}(t)\, J_1(m_2) \exp(j2\pi f_{LO} t) \tag{2}$$

Where f_{LO} is the frequency of the LO signal and m_2 is the LO modulation index. The LO signal output by $EDFA_2$ is divided into three paths by OC_3. Two of the LO signals are shifted to left and right by AOFSs and then sent to the corresponding mixers, and the remaining LO signal is directly sent to the corresponding mixer without frequency shift. Finally, the frequencies of the three LO signals are shown in Fig. 1(a) and can be expressed as

$$\begin{aligned} f_1 &= f_c + f_{LO} - \Delta f_1 \\ f_2 &= f_c + f_{LO} \\ f_3 &= f_c + f_{LO} + \Delta f_2 \end{aligned} \tag{3}$$

Where f_c is the frequency of the optical carrier, the frequency of f_2 is the LO signal without frequency shift, the frequency of f_1 is the LO signal shifted to left through $AOFS_1$, the frequency of f_3 is the LO signal shifted to right through $AOFS_2$. AOFS is based on the Doppler Effect to achieve frequency shift. The advantage is that it does not generate extra optical sidebands and has high energy utilization. The disadvantage is that it can only perform a small range of frequency shift that is typically limited to GHz level. The value of the frequency shift is the bandwidth of the sub-channel. Further more, the frequency shift range of AOFS is not tunable [23], [24].

If there is no IRM and direct mixing, the RF signals in channel 1&4, channel 2&5 and channel 3&6 will have spectrum aliasing after down-conversion as shown in Fig. 1. (b), and they cannot be separated by filters.The schematic diagram of IRM is shown in Fig. 2. It is consists of optical hybrid coupler (OHC),

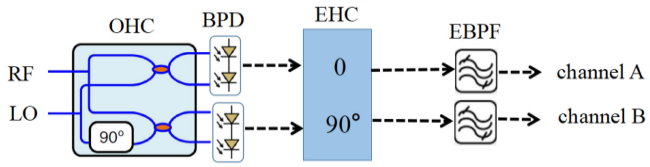

Fig. 2. Schematic diagram of IRM.

balanced photodetector (BPD), electrical hybrid coupler (EHC) and electrical band pass filter (EBPF) [13].

The working principle of the IRM is as follows, when the input RF signal is expressed as $E_{RF}(t) = E_{in}(t)\exp(j\omega_{RF}t)$ and the input LO signal is expressed as $E_{LO}(t) = E_{in}(t)\exp(j\omega_{LO}t)$. The four optical signals output by OHC can be expressed as

$$\begin{aligned} I_1 &= E_{in}(t)\exp(j\omega_{RF}t) + E_{in}(t)\exp(j\omega_{LO}t) \\ I_2 &= E_{in}(t)\exp(j\omega_{RF}t) - E_{in}(t)\exp(j\omega_{LO}t) \\ Q_1 &= E_{in}(t)\exp(j\omega_{RF}t) + jE_{in}(t)\exp(j\omega_{LO}t) \\ Q_2 &= E_{in}(t)\exp(j\omega_{RF}t) - jE_{in}(t)\exp(j\omega_{LO}t) \end{aligned} \quad (4)$$

After BPD, the photocurrent of I and Q can be expressed as

$$\begin{aligned} i_{I(t)} &= 2\eta E_0^2 J_1(m_1)J_1(m_2)\cos(\omega_{RF} - \omega_{LO})t \\ i_{Q(t)} &= 2\eta E_0^2 J_1(m_1)J_1(m_2)sin(\omega_{RF} - \omega_{LO})t \end{aligned} \quad (5)$$

The parameter η represents the responsivity of PD. As shown in Fig. 1(b), the I and Q signals still have the spectrum aliasing of the desired signals and the image interference signals. The amplitudes of these two signals are equal, and the frequency is symmetrical about the LO signal. If the desired signal in the wideband RF signal is expressed as $E_{in}(t)\exp(j\omega_{\mathrm{d}}t)$, ω_{d} is the angular frequency of the desired signal, the image interference signal is expressed as $E_{in}(t)\exp(j\omega_{im}t)$, ω_{i} is the angular frequency of the image interference signal. So there is the following relationship as $\omega_u - \omega_{LO} = -(\omega_{im} - \omega_{LO}) = \omega_{IF}$. The output of EHC can be expressed as

$$\begin{aligned} E_{\mathrm{d}} &= \eta E_0^2 AB\left[\cos\omega_{IF}t + \sin\left(\omega_{IF} + 90^\circ\right)t\right] \\ &= \eta E_0^2 AB\left[\cos\omega_{IF} + \cos\omega_{IF}\right] \\ &= 2\eta E_0^2 AB\cos\omega_{IF} \\ E_i &= \eta E_0^2 AB\left[\cos\omega_{IF}t - \sin\left(\omega_{IF} + 90^\circ\right)t\right] \\ &= \eta E_0^2 AB\left[\cos\omega_{IF} - \cos\omega_{IF}\right] \\ &= 0 \end{aligned} \quad (6)$$

From (6), it can be seen that the image signal is eliminated after EHC.

In this scheme, the input RF signal in the IRM is always the same and is expressed as (1). The input LO signal in the IRM can be expressed as

$$\begin{aligned} E_{LO1}(t) &= 2E_0\exp\left(j2\pi f_c t\right)J_1(m_1)J_1(m_2) \\ &\quad \times \exp(j2\pi f_{LO}t - \Delta f) \\ E_{LO2}(t) &= 2E_0\exp\left(j2\pi f_c t\right)J_1(m_1)\exp(j2\pi f_{LO}t) \\ E_{LO3}(t) &= 2E_0\exp\left(j2\pi f_c t\right)J_1(m_1)J_1(m_2) \\ &\quad \times \exp(j2\pi f_{LO}t + \Delta f) \end{aligned} \quad (7)$$

In (7), $\Delta f_1 = \Delta f_2 = \Delta f$, then, we choose the LO_1 signal which is shifted to the left by Δf through AOFS_1 as an example for the following derivation. The output signals after OHC can be expressed as

$$\begin{aligned} I_1(t) &\propto \mathrm{R}{E_0}^2 J_1(m_1)\cos\left\{2\pi\left[f_{RF}(t) + f_c\right]t \right. \\ &\quad \left. - 2\pi\left(f_{LO} + \Delta f + f_c\right)t\right\}t \\ I_2(t) &\propto -\mathrm{R}{E_0}^2 J_1(m_1)\cos\left\{2\pi\left[f_{RF}(t) + f_c\right]t \right. \\ &\quad \left. - 2\pi\left(f_{LO} + \Delta f + f_c\right)t\right\}t \\ Q_1(t) &\propto \mathrm{R}{E_0}^2 J_1(m_1)\sin\left\{2\pi\left[f_{RF}(t) + f_c\right]t \right. \\ &\quad \left. - 2\pi\left(f_{LO} + \Delta f + f_c\right)t\right\}t \\ Q_2(t) &\propto -\mathrm{R}{E_0}^2 J_1(m_1)\sin\left\{2\pi\left[f_{RF}(t) + f_c\right]t \right. \\ &\quad \left. - 2\pi\left(f_{LO} + \Delta f + f_c\right)t\right\}t \end{aligned} \quad (8)$$

The output signals after BPD can be expressed as

$$\begin{aligned} I(t) &\propto 2\mathrm{R}{E_0}^2 J_1(m_1)\cos\left\{2\pi\left[f_{RF}(t) + f_c\right]t \right. \\ &\quad \left. - 2\pi\left(f_{LO} + \Delta f + f_c\right)t\right\}t \\ Q(t) &\propto 2\mathrm{R}{E_0}^2 J_1(m_1)\sin\left\{2\pi\left[f_{RF}(t) + f_c\right]t \right. \\ &\quad \left. - 2\pi\left(f_{LO} + \Delta f + f_c\right)t\right\}t \end{aligned} \quad (9)$$

When $I(t)$ and $Q(t)$ are combined by an EHC, the desired IF signal and the image interference signal could be separated, as shown in Fig. 1(c)–(d). Therefore, the two output ports of the IRM are the channel 1 and channel 4 respectively. Because the frequency of the input LO signal is different in corresponding IRMs, so are the output sub-channels from the IRMs.

III. Experiment and Result

A continuous light wave with the frequency of 193.515 THz and the power of 17 dBm is generated by an LD (RIO, 01075-0.2-004) and split into two equal branches by OC_1. In the upper branch, the optical carrier is sent to MZM_1 (SUMITOMO, T. MXH1.5-40) and is modulated by a wideband RF signal that is generated by a vector signal source (Agilent, E8267C). The MZM_1 works at the minimum transmission point (MITP) with a half-wave voltage of 3.5V and the insertion loss of 6dB. The $+1$st order optical sideband of the RF modulated signal is amplified by EDFA_1 (Keopsys, KPS-STD-BT-C-19-HG) and then split into three branches by OC_2 before being sent to OHCs (Kylia COH24).

In the lower branch, the optical carrier is modulated by the LO signal in MZM_2 (EOspace AX-DV5-40-PFV-SFV). The half-wave voltage of MZM_2 is 4V, and the insertion loss is 4 dB.

The CS-DSB signal generated by MZM_2 is shown in Fig. 3(a) and the $+1$st order sideband selected by OBPF_2 (Finisar 16000S) is shown in Fig. 3(b). The LO signal, generated by a microwave signal source (Agilent E8257D), has a frequency of 23 GHz and a power of 10 dBm. The $+1$st order optical sideband of the RF modulated signal is amplified by EDFA_2

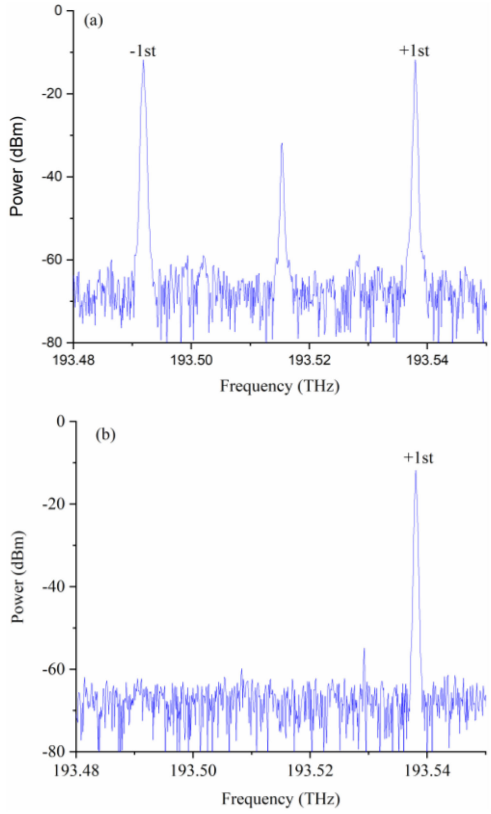

Fig. 3. Measured optical spectra of LO modulated signal.

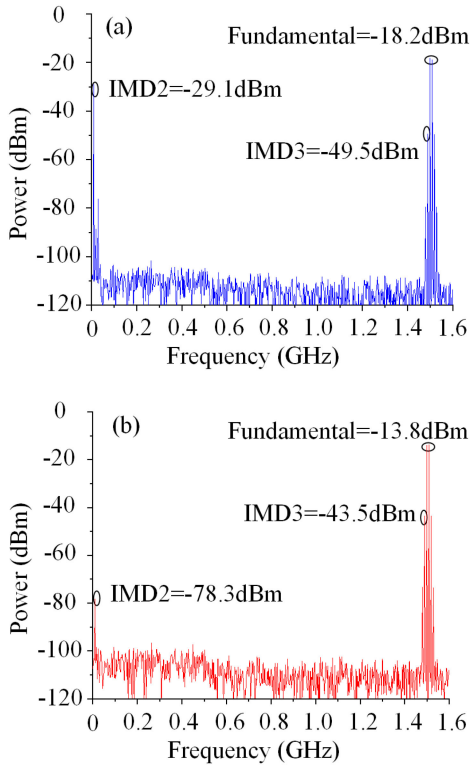

Fig. 4. IF spectrum. (a) Without balanced detection. (b) With balanced detection.

(Keopsys, CEFA-C-PB-HP) and then split into three branches by OC_3. In the first branch, the LO signal is shifted to the left by 1 GHz through the $AOFS_1$ (IPF-1000-1550-3FP) and is defined as LO_1. In the second branch, the LO signal without frequency shift is defined as LO_2. In the third branch, the LO signal is shifted to the right by 1 GHz through the $AOFS_2$ and is defined as LO_3. It should be noted that the frequency shift direction and frequency shift range of each AOFS are fixed and non-adjustable. For example, $AOFS_1$ in this scheme can only shift the frequency to the left by 1 GHz, while $AOFS_2$ can only shift the frequency to the right by 1 GHz.

In order to improve the SFDR of the system by suppressing the second-order intermodulation distortion (IMD2), a balanced detection technology is used in this scheme. Two-tone signals with the frequencies of 24.5 and 24.51 GHz and the power of 0 dBm are used as the input RF signals. The frequency of the LO signal is 23 GHz and the power is 10 dBm. After down-conversion, the frequencies of the two fundamental terms are 1.5 GHz and 1.51 GHz, the third-order intermodulation distortion (IMD3) frequencies are 1.49 GHz and 1.52 GHz, and the second-order intermodulation distortion (IMD2) frequency is 10 MHz. Fig. 4 shows the intermediate frequency (IF) spectrum with or without balance detection after down-conversion.

Fig. 4(a) shows the measurement result without balanced detection, it can be seen that the power of IMD2 at this time is −29.1 dBm as the main distortion. Although the frequency of IMD3 is closer to the fundamental terms, its power is relatively small so the distortion effect on the system is also limited. Fig. 4(b) shows the measurement result with balanced detection, the power of IMD2 is reduced from −29.1 dBm to −78.3 dBm, which is suppressed by 49.2 dBm, and the fundamental term are improved by 4.4 dB after balanced detection.

The SFDR is also measured by using the above two-tones signals and LO signal. The power of input RF signal is changed from -15 to 30 dBm, and the power of fundamental term, IMD2, IMD3 and noise floor are measured respectively. Fig. 5(a) shows the result without balanced detection, although SFDR3 can reach 101.8 $dB{\cdot}Hz^{2/3}$, the overall SFDR of the system, limited by SFDR2, can only reach 72.3 $dB{\cdot}Hz^{1/2}$. When the balanced detection is performed, SFDR3 is changed from 101.8 $dB{\cdot}Hz^{2/3}$ to 103.2 $dB{\cdot}Hz^{2/3}$, with 1.4 dB improved. What is more important, the SFDR2 is changed from 72.3 $dB{\cdot}Hz^{1/2}$ to 96.1 $dB{\cdot}Hz^{1/2}$, which means the overall SFDR of the system is improved by 23.8 dB.

The dual-output image rejection is also performed in the proposed scheme. When the RF signal is at 20-21 GHz, it is received by channel 1, and when the RF signal is at 23-24 GHz, it is received by channel 4. The channel 1 and channel 4 are image interference signals of each other and can be output from the two output ports of the EHC.

First, the image rejection test is performed on channel 1 and channel 4. When the frequency of the LO signal is 22 GHz, two-tone signals with frequencies of 20 GHz, 20.2 GHz, 20.4 GHz, 20.6 GHz and 20.8 GHz are used as RF signals for frequency down conversion. Meanwhile, two-tone signals with frequencies of 23.2 GHz, 23.4 GHz, 23.6 GHz, 23.8 GHz and 24 GHz are

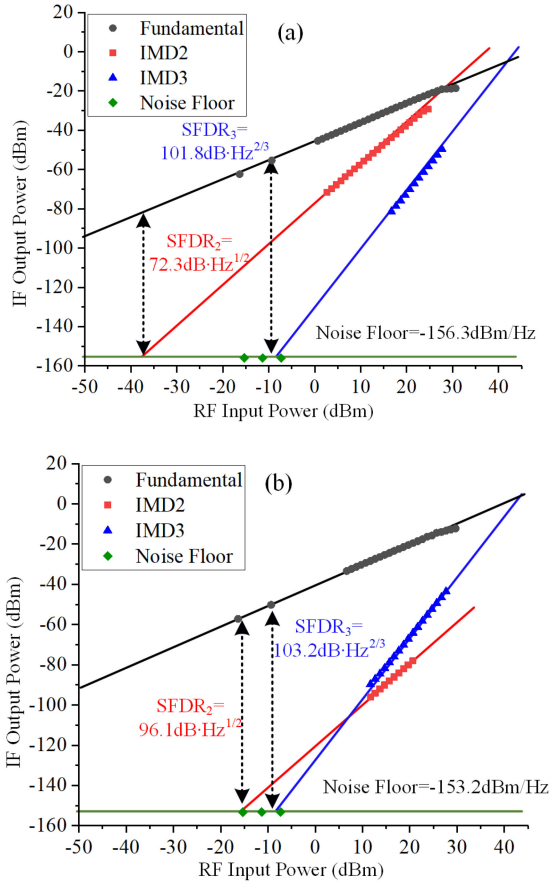

Fig. 5. SFDR measurement. (a) Without balanced detection. (b) With balanced detection.

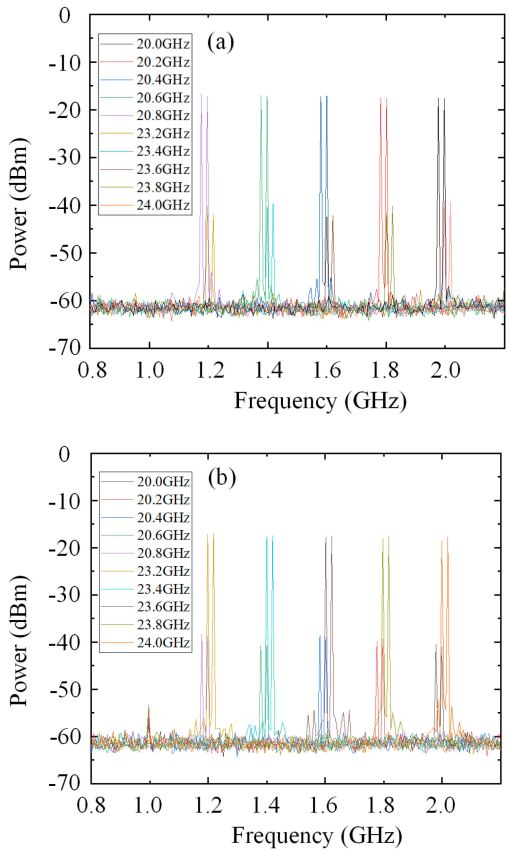

Fig. 6. Results of image rejection. (a) Channel 1 as the main channel. (b) Channel 4 as the main channel.

used as image interference signals. The down converted IF signal is shown in Fig. 6, which respectively represent the electrical spectrum of the two output ports of the EHC. It can be seen that the image rejection ratio is around 25 dB. Similarly, the measurement results of the other 4 channels are shown in Fig. 7.

We measured the amplitude response of channel 1 through experiments. When the input power of the RF signal is constant, the frequency of RF signal are changed from 20 GHz to 21 GHz with a step of 50 MHz. The power of IF signals are measured, as shown in Fig. 8. It can be seen that the jitter amplitude of the IF signal is less than 2 dB, which means that channel 1 has a flat amplitude response. That is because the components used in the microwave photonic channelized receiver include optical devices and electrical devices. The 3 dB bandwidth of optical devices is generally large, but the 3 dB bandwidth of electrical devices is relatively small. Therefore, the sub-channel amplitude response of the channelizer is mainly limited by the amplitude-frequency response of the electric microwave devices in the system such as the EHC. These devices have serious frequency dependence at high frequencies. The amplitude measurement results of the other 5 sub-channels are similar to channel 1.

Channelized receivers based on dual optical combs usually have the effect of channel crosstalk, and the channel crosstalk is mainly caused by the residual optical carrier and optical sidebands that are not completely filtered out by the OBPF. This scheme is based on Doppler frequency shift and will not produce other optical sidebands, so it is hardly affected by channel crosstalk.

Error vector magnitude (EVM) is an important parameter that can comprehensively manifests the amplitude error and phase error of the modulation signal. The better the EVM and constellation diagram, the better the signal quality obtained after demodulation, which also demonstrates that the proposed channelized receiver can channelize the wideband RF signal and restore the modulated microwave signal carried by RF carrier. After channelization, the frequency of down-converted IF signal is demodulated by the vector signal analyzer and the constellation diagram is obtained to evaluate its signal quality. Therefore, the minimum value of EVM is the best point of communication.There are many factors that affect EVM, such as the nonlinear distortion of the link. In order to further study the influence of the power of the input signal on the EVM, we used a 16QAM signal with a center frequency of 22 GHz and a bit rate of 100 MBaud for measurement. The constellation diagram shown in Fig. 9(a) is obtained by direct demodulation of the vector signal generated by the vector signal source and the EVM is 2.4%. The constellation diagram and EVM in the proposed scheme are measured and shown in Fig. 9(b). When the power of RF signal changes from −25 dBm to 5 dBm, the EVM gradually decreases and then stabilizes to the minimum EVM point about 4.7%. The drop in EVM is caused by changes in the

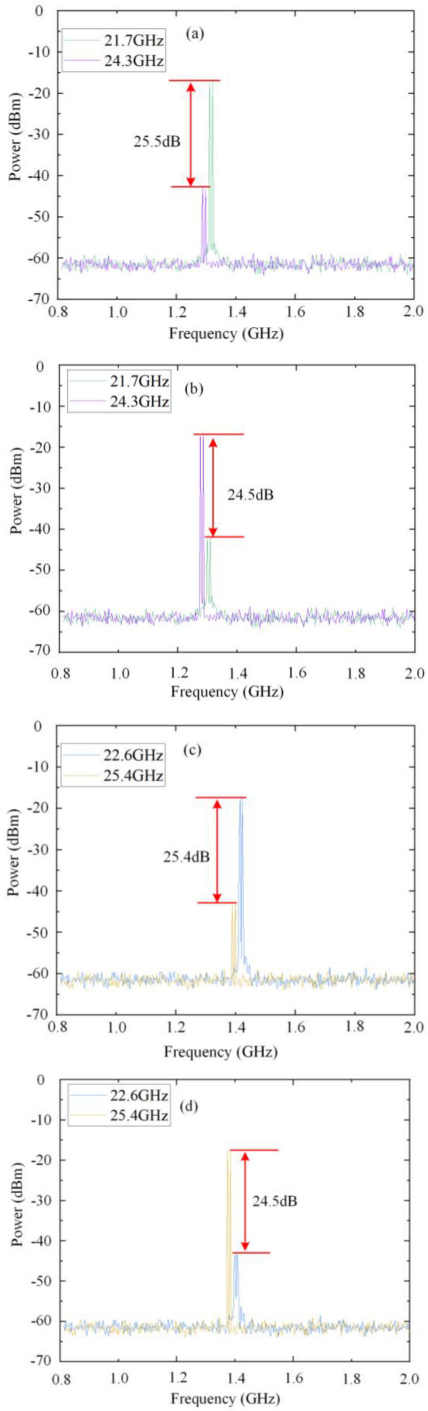

Fig. 7. Results of image rejection. (a) Channel 2 as the main channel. (b) Channel 5 as the main channel. (c) Channel 3 as the main channel. (d) Channel 6 as the main channel.

signal to noise ratio (SNR), and the minimum point of the EVM is also the maximum point of the SNR. When the power of RF signal changes from 5 dBm to 15 dBm, the EVM becomes larger and the constellation diagram becomes worse. At this time, due to the increase in the amplitude of the high-order optical sidebands, high-order intermodulation distortion has become the main reason for the deterioration of EVM.

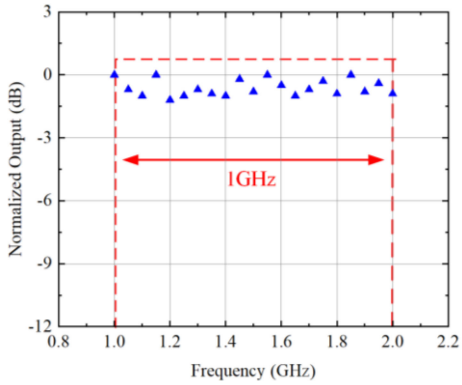

Fig. 8. Measured amplitude response of channel 1.

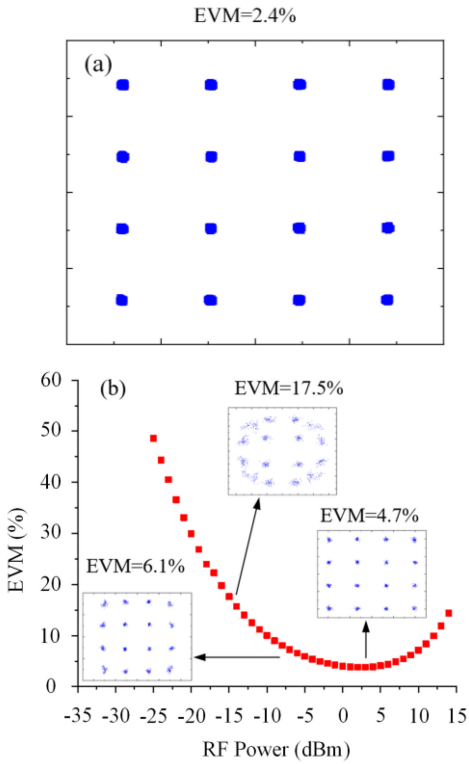

Fig. 9. Measured the photonic integration technology and constellation diagram. (a) Direct demodulation. (b) Demodulation after microwave photonic link.

IV. Conclusion

In this paper, a novel microwave photonic channelizer based on AOFS is proposed and demonstrated. A broadband RF signal covering 20-26 GHz is sliced into six sub-channels for reception, the scheme we proposed does not need to use any OFC, so it has the advantages of simple structure, easy implementation, and minimal channel crosstalk. With a photonic dual-output IRM based on the balanced Hartley structure, only three IRMs are needed to output six sub-channels. The in-band interference suppression ratio is about 25 dB and the SFDR is about 96.1 $dB \cdot Hz^{1/2}$. If we want to expand the number of sub-channels, we can use an n-lines OFC to replace the single LO signal, and then shift the OFC left and right to obtain a number of 3n LO

signals, so as to achieve the number of 6n sub-channel reception. The proposed scheme can find applications in RF systems with high operational frequency and a large instantaneous bandwidth for radars, communications, and electrical warfare.

REFERENCES

[1] X. J. Xie *et al.*, "Broadband photonic RF channelization based on coherent optical frequency combs and I/Q demodulators," *IEEE Photon. J.*, vol. 4, no. 4, pp. 1196–1202, Aug. 2012.

[2] P. Rugeland, Z. Yu, C. Sterner, G. Tarasenko, and W. Margulis, "Photonic scanning receiver using an electrically tuned fiber bragg grating," *Opt. Lett.*, vol. 34, no. 24, pp. 3794–3796, 2009.

[3] J. H. Wo *et al.*, "Dual-passband microwave photonic filter for fiber axial strain measurement," in *Porc. 16th Int. Opt. Comm. Networ. Conf.*, China, 2017, pp. 1–3.

[4] Q. Wang, L. Huo, and Y. F. Xing, "Ultra-flat optical frequency comb generator using a single-driven dual-parallel Mach-Zehnder modulator," *Opt. Lett.*, vol. 39, no. 10, pp. 3050–3053, 2014.

[5] L. X. Wang *et al.*, "Polarization division multiplexed photonic radio-frequency channelizer using an optical comb," *Opt. Commun.*, vol. 286, no. 1, pp. 282–287, 2013.

[6] F. Imon *et al.*, "GPU synthesis of RF channeliser outputs for a variable bandwidth microwave digital receiver," in *Porc. 12th Int. Signal. Proc. Comm. Syst. Conf.*, Australia, 2018, pp. 1–8.

[7] D. Zhu and S. L. Pan, "Broadband cognitive radio enabled by photonics," *J. Lightw. Technol.*, vol. 38, no. 12, pp. 3076–3088, 2020.

[8] X. S. Meng *et al.*, "Tunable photonic microwave frequency down-converter using opto-electronic oscillator based on integrated three-section laser," in *Porc. 20th Int. Comm. Technol. Consf.*, China, 2020, pp. 998–1001.

[9] Y. H. Chong and X. H. Li, "A microwave photonic channelization device with common intermediate frequency," *J. Optoelectron.·Laser*, vol. 25, no. 12, pp. 2294–2299, 2014.

[10] W. H. Hao, Y. T. Dai, and K. Xu, "Chirped-pulse-based broadband RF channelization implemented by a mode-locked laser and dispersion," *Opt. Lett.*, vol. 42, no. 24, pp. 5234–5237, 2017.

[11] Z. Z. Tang and S. L. Pan, "Image-reject mixer with large suppression of mixing spurs based on a photonic microwave phase shifter," *J. Lightw. Technol.*, vol. 34, no. 20, pp. 4729–4735, 2016.

[12] X. Y. Xu *et al.*, "Broadband photonic RF channelizer with 92 channels based on a soliton crystal microcomb," *J. Lightw. Technol.*, vol. 38, no. 18, pp. 5116–5121, 2020.

[13] Z. Z. Tang and S. L. Pan, "A reconfigurable photonic microwave mixer using a 90° optical hybrid," *IEEE Trans. Microw. Theory Tech.*, vol. 64, no. 9, pp. 3017–3025, Sep. 2016.

[14] Z. Z. Tang, D. Zhu, and S. L. Pan, "Coherent optical RF channelizer with large instantaneous bandwidth and large in-band interference suppression," *J. Lightw. Technol.*, vol. 36, no. 19, pp. 4219–4226, 2018.

[15] D. Marpaung, J. P. Yao, and J. Capmany, "Integrated microwave photonics," *Nature Photon.*, vol. 13, no. 3, pp. 80–90, Feb. 2019.

[16] Y. Liu, A. Choudhary, D. Marpaung, and B. J. Eggleton, "Integrated microwave photonic filters," *Adv. Opt. Photon.*, vol. 12, no. 2, pp. 485–555, Jun. 2020.

[17] Y. S. Gao, A. Wen, W. Zhang, W. Jiang, J. Ge, and Y. Fan, "Ultra-wideband photonic microwave I/Q mixer for zero-IF receiver," *IEEE Trans. Microw. Theory Tech.*, vol. 65, no. 11, pp. 4513–4525, Nov. 2017.

[18] P. X. Li *et al.*, "All-optical and broadband microwavefundamental/sub-harmonic I/Q down-converters," *Opt. Exp.*, vol. 26, no. 6, pp. 7336–7350, Feb. 2018.

[19] S. T. Lipkowitz, T. U. Horton, and T. E. Murphy, "Wideband microwave electro-optic image rejection mixer," *Opt. Lett.*, vol. 44, no. 19, pp. 4710–4713, 2019.

[20] B. Yang, H. Chi, S. Yang, Z. Cao, J. Ou, and Y. Zhai, "Broadband microwave spectrum sensing based on photonic RF channelization and compressive sampling," *IEEE Photon. J.*, vol. 12, no. 1, pp. 1–9, Feb. 2020.

[21] X. Y. Xu, M. X. Tan, J. Y. Wu, R. Morandotti, A. Mitchell, and D. J. Moss, "Microcomb-based photonic RF signal processing," *IEEE Photon. Technol. Lett.*, vol. 31, no. 23, pp. 1854–1857, Dec. 2019.

[22] A. L. Gaeta, M. Lipson, and T. J. Kippenberg, "Photonic-chip-based frequency combs," *Nature Photon.*, vol. 13, no. 3, pp. 158–169, Mar. 2019.

[23] H. G. C. Chatellus, L. R. Cortés, C. Schnébelin, M. Burla, and J. Azaña, "Reconfigurable photonic generation of broadband chirped waveforms using a single CW laser and low-frequency electronics," *Nature Photon.*, vol. 2018, no. 1, pp. 1–12, 2018.

[24] C. Schnébelin and H. G. C. Chatellus, "Agile photonic fractional fourier transformation of optical and RF signals," *Opt.*, vol. 4, no. 8, pp. 907–910, Aug. 2017.